MAGIC: Mosaic Analysis by gRNA-Induced Crossing-over

Sarah E. Allen[1,3], Gabriel T. Koreman[1,2,3], Ankita Sarkar[1,2,3], Bei Wang[1,2], Mariana F. Wolfner[1,4], and Chun Han[1,2,4]

[1]Department of Molecular Biology and Genetics, Cornell University, Ithaca, NY 14853, USA

[2]Weill Institute for Cell and Molecular Biology, Cornell University, Ithaca, NY 14853, USA

[3]These authors contributed equally to this work, listed alphabetically

[4]For correspondence: mariana.wolfner@cornell.edu (MFW) and chun.han@cornell.edu (CH)

Abstract:

Mosaic animals have provided the platform for many fundamental discoveries in developmental biology, cell biology, and other fields. Techniques to produce mosaic animals by mitotic recombination have been extensively developed in *Drosophila melanogaster* but are less common for other laboratory organisms. Here, we report mosaic analysis by gRNA-induced crossing-over (MAGIC), a new technique for generating mosaic animals based on DNA double-strand breaks produced by CRISPR/Cas9. MAGIC efficiently produces mosaic clones in both somatic tissues and the germline of *Drosophila*. Further, by developing a MAGIC toolkit for one chromosome arm, we demonstrate the method's application in characterizing gene function in neural development and in generating fluorescently marked clones in wild-derived *Drosophila* strains. Eliminating the need to introduce recombinase-recognition sites in the genome, this simple and versatile system simplifies mosaic analysis in *Drosophila* and can be applied in any organism that is compatible with CRISPR/Cas9.

Keywords: *MAGIC*, *mosaic analysis, CRISPR/Cas9, gRNA, clonal analysis, germline, imaginal disc, da neurons, Drosophila dominant female sterility,*

26 **Introduction:**

27 Mosaic animals contain genetically distinct populations of cells that have arisen from one
28 zygote. Mosaic animals have historically played important roles in the study of pleiotropic genes,
29 developmental timing, cell lineage, neural wiring, and other complex biological processes. Given
30 its genetic tractability, *Drosophila* has been a major system for generating and studying such
31 mosaics (Perrimon, 1998), which have led to important discoveries such as developmental
32 compartments (Garcia-Bellido et al., 1976), cell autonomy (Heitzler and Simpson, 1991), and
33 maternal effects of zygotic lethal genes (Perrimon et al., 1989). Mosaic (also called clonal)
34 analysis is currently used to study tumor suppressors (Feng and Irvine, 2007), signaling
35 pathways (Huang et al., 2014), sleep-wake behaviors (Chung et al., 2017), cell fates (Hu and
36 Jasper, 2019), and neuronal lineages (Lee, 2014), among other biological processes.

37 The earliest mosaic analyses relied on spontaneous mitotic recombination (Stern, 1936),
38 rare events in which a DNA double-strand break (DSB) during the G_2 phase of the cell cycle is
39 repaired by homologous recombination, resulting in the reciprocal exchange of chromosomal
40 arms between homologous chromosomes distal to the site of the DNA crossover (reviewed in
41 Griffin et al., 2014). Ionizing radiation, such as X-rays (Muller, 1928), cause DSBs and thus
42 were later used in *Drosophila* to increase the baseline level of mitotic recombination (Xu and
43 Rubin, 2012). However, ionizing radiation breaks genomic DNA at random locations and is
44 associated with a high degree of lethality.

45 To overcome these limitations, the yeast Flippase (Flp)/FRT system was introduced into
46 *Drosophila* to mediate site-specific recombination at FRT sites (Golic and Lindquist, 1989; Xu
47 and Rubin, 1993), enabling the development of an ever-expanding toolbox with enhanced
48 power and flexibility for clonal analysis (Griffin et al., 2009; Harrison and Perrimon, 1993; Lee
49 and Luo, 1999; Xu and Rubin, 1993; Yu et al., 2009). This system requires that both
50 homologous chromosomes carry FRT sites at the same position proximal (relative to the
51 centromere) to the gene of interest, and an independent marker on one of the homologs to allow

52 visualization of the genetically distinct clones (Xu and Rubin, 1993). For clonal analysis in the
53 *Drosophila* germline, a dominant female sterility (DFS) *ovo*^{D1} transgene was combined with
54 Flp/FRT methods, allowing production of, and selection for, germline clones homozygous for a
55 mutation of interest in a heterozygous mother (Chou and Perrimon, 1992; Perrimon and Gans,
56 1983). In this "Flp-DFS" technique, egg production from *ovo*^{D1}-containing heterozygous and
57 homozygous germline cells is blocked, resulting in progeny derived exclusively from germline
58 clones lacking *ovo*^{D1} that were generated by mitotic recombination (Chou et al., 1993). Clonal
59 analysis based on somatic recombination has also been achieved in mice using the Cre-LoxP
60 system and the reconstitution of fluorescent protein genes as markers (Henner et al., 2013;
61 Zong et al., 2005). Despite these successes, site-specific recombination systems have not been
62 widely used for mitotic recombination in model animals beyond *Drosophila melanogaster* due to
63 the challenging task of introducing recombinase-recognition sites into centromere-proximal
64 regions for every chromosome.

65 Given the power of mosaic animals in biological research, it would be useful to have a more
66 general approach for inducing interhomolog mitotic recombination in any organism,
67 circumventing the challenges just mentioned. The CRISPR/Cas9 system has great potential for
68 extending clonal analysis, because it can create targeted DSBs in the genomic DNA of a wide
69 array of organisms (Sander and Keith Joung, 2014). This binary system requires only the Cas9
70 endonuclease and a guide RNA (gRNA) that specifies the DNA target site (Jinek et al., 2012),
71 both of which can be introduced into the cell independently of the location of the target site.
72 CRISPR/Cas9-induced DSBs can be repaired either by non-homologous end joining (NHEJ) or
73 homology-directed repair (HDR). So far, most CRISPR/Cas9 applications in animals have been
74 focused on NHEJ-mediated mutagenesis and HDR-mediated gene replacement (Salsman and
75 Dellaire, 2017), and CRISPR/Cas9-induced mitotic recombination has not been demonstrated in
76 multicellular organisms. Here, we report mosaic analysis by gRNA-induced crossing-over
77 (MAGIC), a novel CRISPR/Cas9-based technique for clonal analysis. This method can be used

78 to generate mosaic clones in both the *Drosophila* soma and germline. Based on this method, we
79 built a convenient toolkit to generate and label mosaic clones for genes located on chromosome
80 arm 2L. We demonstrate the success of our toolkit for clonal analysis in the soma and the
81 germline and show its applications in analyzing gene functions in neuronal dendrite
82 development. Lastly, we also demonstrate that MAGIC can be used successfully with unmarked
83 wild-derived strains, indicating that this method can be extended to organisms beyond
84 *Drosophila*.

85 **Results:**

86 ***Rationale for MAGIC***

87 MAGIC relies on the action of gRNA/Cas9 in a proliferating cell during G_2 phase to generate a
88 DSB at a specific position on one chromatid of a homologous pair (Figure 1A). The DSB can
89 induce a crossover between this chromatid and a chromatid from the homologous chromosome,
90 resulting in exchange of chromosome segments between the two chromatids at the location of
91 the DSB. During the subsequent mitotic segregation of chromosomes, a 50% chance exists for
92 identical distal chromosome segments to sort into the same daughter cells, generating "twin
93 spots", which contain two genetically distinct populations of cells homozygous for the
94 chromosome segment distal to the exchange.

95 ***Using CRISPR-induced crossover to generate clones in the* Drosophila *soma and***
96 ***germline***

97 For our initial tests of the ability of MAGIC to generate mosaic clones in somatic tissues, we
98 used ubiquitously expressed gRNAs to induce DSBs at the *gnu* locus and a ubiquitous
99 fluorescent marker, *His2Av-GFP* (Clarkson and Saint, 1999), to trace clones (Figure 1B). Both
100 *His2Av-GFP* and *gnu* are located on the left arm of chromosome 3 (3L), and *His2Av-GFP* is
101 distal to *gnu*. We chose *gnu* as our gRNA target because we have already made an efficient
102 *gRNA-gnu* line for other purposes (to be published elsewhere); furthermore, this gene is only
103 required maternally for embryonic development (Freeman et al., 1966), so mutations of *gnu* are

104 not expected to affect the viability or growth of somatic cells. We induced clones using three
105 different Cas9 transgenes, each of which is expressed in the developing wing disc under the
106 control of a different enhancer. With all three Cas9s, we observed twin spots consisting of bright
107 *His2Av-GFP* homozygous clones abutting GFP-negative clones in the midst of *His2Av-GFP/+*
108 heterozygous cells (Figures 1C-1E) in every imaginal disc examined, demonstrating the
109 feasibility of MAGIC for generating somatic mosaics.

110 Given that CRISPR/Cas9 is active in both the soma and the germline of *Drosophila*
111 (Gratz et al., 2013; Port et al., 2014; Ren et al., 2013), we next tested for MAGIC clone induction
112 in the germline by using the DFS technique and the germline-specific *nos-Cas9* (Port et al.,
113 2014) (Figure S1A). We used an ovo^{D1} transgene located on chromosome arm 2R and induced
114 DSBs at the *Rab3* locus, which is located on the same arm proximal to the location of ovo^{D1}
115 (Figure 1F). Since *Rab3* is a non-essential gene expressed only in neurons (Chen et al., 2015),
116 its disruption in the female germline should affect neither egg production nor embryonic
117 development of the progeny. Due to the dominant effect of ovo^{D1}, restoration of egg production
118 can only result from mitotic recombination proximal to ovo^{D1} (e.g. at *Rab3* in this case), followed
119 by generation of ovo^{D1} negative clones. As expected, control females that contained ovo^{D1} and
120 *nos-Cas9*, but not *gRNA-Rab3*, did not produce any eggs. In contrast, most females carrying all
121 three components produced 20-90 eggs each (Figure 1G), many of which hatched into larvae
122 (Figure 1H), suggesting successful mitotic recombination.

123 The results above together show that, like the Flp/FRT system, MAGIC is an effective
124 approach for generating homozygous clones via mitotic recombination in both *Drosophila* soma
125 and germline.

126 ***A toolkit for generating labeled clones for genes on chromosome arm 2L***

127 Towards making MAGIC a general approach for analyzing *Drosophila* genes, we built a toolkit
128 for genes located on chromosome arm 2L as a proof-of-principle. We designed transgenic
129 constructs that each integrate two features simultaneously: ubiquitously-expressed gRNAs that

130 target a pericentromeric region and a ubiquitously-expressed marker for labeling clones. The
131 constructs were inserted into a distal position of 2L. When used together with an unmodified 2nd
132 chromosome, they label clones homozygous for nearly the entirety of the unmodified arm either
133 negatively or positively. Negative labeling in the nMAGIC option is achieved by expressing a
134 nuclear blue fluorescent protein (nBFP) reporter such that clones homozygous for the
135 unmodified arm lose nBFP expression (Figure 2A). Positive labeling with pMAGIC utilizes a
136 Gal80 marker (Lee and Luo, 1999), which suppresses Gal4-driven expression of a fluorescent
137 reporter (Figure 2B). Therefore, only the cells that lose Gal80 transgene will be fluorescently
138 labeled, similarly to mosaic analysis with a repressible cell marker (MARCM) (Lee and Luo,
139 1999).

140 To identify appropriate gRNA target sites, we surveyed the pericentromeric sequences
141 of 2L for sequences that met three criteria: (1) being reasonably conserved so that DSBs can be
142 induced in most *Drosophila* strains; (2) not functionally critical and being distant from essential
143 sequences so that indel mutations in nearby regions would not disrupt important biological
144 processes; and (3) unique in the genome, so as to avoid off-target effects. Therefore, for each
145 MAGIC construct, we chose a pair of non-repeat gRNA target sequences in an intergenic region
146 to enhance the chance of DSBs. The two gRNA target sequences are closely-linked to reduce
147 the risk of large deletions (Figure 2C). In addition, we preferentially chose sequences that are
148 conserved among closely related *Drosophila* species (*D. melanogaster*, *D. simulans*, and *D.*
149 *sechellia*) but not in more distant species. Considering the varying efficiencies of different gRNA
150 target sequences, we selected three pairs of gRNAs targeting three chromosomal locations
151 (40D2, 40D4, and 40E1) and tested their ability to produce clones in wing discs, neurons, and
152 the germline.

153 Clones were induced in a specific tissue by a Cas9 transgene that is expressed in
154 precursor cells of that tissue. We used *hh-Cas9* (Poe et al., 2019) for nMAGIC in the wing
155 imaginal disc (Figure 2D), *SOP-Cas9* (Poe et al., 2019) for pMAGIC in larval class IV dendritic

156 arborization (C4da) sensory neurons (Figure 2F), and *nos-Cas9* for the female germline (Figure
157 S1B). gRNAs targeting 40D2 consistently performed the best in generating clones in wing discs
158 and C4da neurons (Figures 2E and 2G) and appear to be the most efficient in the germline,
159 even though the differences in the germline were not statistically significant (Figures 2H and 2I).
160 Although the overall efficiencies of *gRNA-40D2* and *gRNA-40D4* in inducing clones in da
161 neurons are similar (Figure 2G and Figure S2A), *gRNA-40D4* induced more clones in a different
162 type of neuron (class III). The fact that the three gRNA pairs showed similar trends in their ability
163 to induce clones across different tissues suggests that an efficient gRNA construct for one
164 tissue will likely perform well in other tissues also. These results indicate that we have created
165 an efficient MAGIC toolkit for genes located on chromosome arm 2L. Analogous toolkits could
166 easily be made for any other chromosome arm, using the same methods.

167 ***Clonal analysis of neuronal dendrite development***

168 To evaluate the utility of our MAGIC toolkit for characterizing gene function at the single-cell
169 level, we combined the pMAGIC line *gRNA-40D2(Gal80)* with mutations on 2L that affect
170 dendrite morphogenesis in C4da neurons by disrupting vesicular trafficking. We first used two
171 genes, *Secretory 5* (*Sec5*) (Peng et al., 2015) and *Rab5* (Satoh et al., 2008), that have been
172 shown to be required for dendrite growth. We observed dendrite reduction in C4da clones
173 carrying homozygous mutations in these genes (Figures 3A and 3B), recapitulating previously
174 published results using MARCM with the same mutants (Peng et al., 2015; Satoh et al., 2008).
175 A third gene, *Syntaxin 5* (*Syx5*), was identified in our unpublished RNAi screens. Clones
176 carrying a null mutation of *Syx5* produced the most dramatic dendrite reduction, with almost all
177 terminal dendrites eliminated (Figure 3C), consistent with the expected role of Syx5 in ER to
178 Golgi vesicle trafficking (Hardwick and Pelham, 1992). Therefore, our MAGIC reagents for 2L
179 can be used to characterize gene functions in single cells with a power analogous to that of
180 MARCM but with a much simpler system.

181 ***Generation of clones by MAGIC in fly lines with wild-derived genomes***

182 A substantial advantage of MAGIC compared to Flp/FRT-based mitotic recombination systems
183 is that MAGIC does not require prior genetic modification of the chromosome arm to be tested.
184 It therefore has the potential to be applied to fly strains with wild-derived genomes, and even
185 other organisms. To test the applicability of MAGIC to unmarked strains with wild-derived
186 genomes, we crossed *gRNA-40D2(nBFP); hh-Cas9* to five randomly chosen lines from the
187 *Drosophila* Genetic Reference Panel (DGRP) (MacKay et al., 2012), a set of standard strains
188 established from flies captured in the wild. In all cases, we observed efficient clone induction in
189 wing imaginal discs (Figures 4A-4E), demonstrating the potential of MAGIC for clonal analysis
190 of the function of natural alleles residing on wild-derived chromosomes.

191 **Discussion:**

192 We present here a new technique we name MAGIC (mosaic analysis by gRNA-induced
193 crossing-over) for clonal analysis based on CRISPR-induced mitotic recombination. We show
194 that MAGIC is capable of producing efficiently mosaic tissues in both the *Drosophila* soma and
195 germline, using gRNAs targeting various chromosomal locations. Integrated gRNA-marker
196 constructs enable both positive- and negative-labeling of homozygous clones. As demonstrated
197 by our 2L toolkit, MAGIC is simple and effective to use; similar MAGIC reagents can be
198 generated easily for all other chromosome arms to allow for genome-wide characterization of
199 gene functions.

200 Although conventional Flp/FRT-based techniques have been widely and successfully
201 used in *Drosophila* for similar clonal analyses (Griffin et al., 2014), MAGIC has two major
202 advantages. The first is the simplicity of MAGIC assays: This system eliminates the requirement
203 for genetic modification of the test chromosome; furthermore, integrating gRNAs and genetic
204 markers into one transgenic construct further reduces the number of necessary genetic
205 components. Therefore, gRNA-marker transgenes can be combined with existing mutant
206 libraries to perform MAGIC with very little additional effort. The second advantage of MAGIC is
207 that mitotic recombination is not limited by the available FRT insertion sites. While introducing

208 FRT to a specific pericentromeric region is very difficult and historically required labor-intensive
209 genetic screens, CRISPR/Cas9 can induce DNA DSBs and subsequent crossover at specific
210 pericentromeric sequences with ease. Therefore, MAGIC opens doors for clonal analysis of
211 genes that were previously impossible to study using existing FRT sites, such as those on the
212 fourth chromosome and the ones near centromeres. In addition, many *Drosophila* mutations are
213 associated with transgenic constructs containing FRT (Thibault et al., 2004), making analyses
214 complicated when using Flp/FRT-based techniques. In contrast, MAGIC should be compatible
215 with all of these gene disruption lines.

216 The unique mechanism of MAGIC requires three considerations for successful
217 applications. First, our results suggest that the gRNA target sequence strongly influences the
218 efficiency of clone induction, likely by affecting the frequency of DNA DSBs in premitotic cells.
219 Therefore, for clonal analysis of a specific chromosomal arm, it is beneficial to compare a few
220 candidate gRNA targets and select the most effective one. Second, because perfect DSB repair
221 will recreate the gRNA target site and allow for one more round of Cas9 cutting, most cells that
222 have expressed Cas9 in their lineages are expected to eventually harbor indel mutations that
223 disrupt the gRNA target site, regardless of whether or not the DSBs have led to mitotic
224 recombination. However, this caveat can be mitigated by choosing gRNA sites in non-critical
225 sequences, which can be validated by crossing gRNA lines to a ubiquitous Cas9 or by
226 comparing gRNA-induced control clones to wildtype cells. Lastly, since only DNA DSBs in the
227 G_2 phase can lead to clone generation, the timing of Cas9 action is expected to be critical for
228 MAGIC. For the cell type in question, an ideal Cas9 should be expressed in the precursor cells,
229 as too early expression can mutate gRNA target sites prematurely and too late expression will
230 lead to unproductive DSBs.

231 Perhaps the most exciting aspect of MAGIC is its potential for use with wild-derived
232 *Drosophila* strains and in organisms beyond *Drosophila*. DGRP wild-derived strains have played
233 important roles in identification of natural alleles that are associated with certain phenotypic

234 variations (Clark et al., 1994; Grenier et al., 2015; Mackay and Huang, 2018; Shorter et al.,
235 2015). However, it has been difficult to investigate the effect of homozygosity for alleles within
236 these strains without being able to use available genetic tools (e.g. Gal4 drivers and fluorescent
237 markers) in *Drosophila*. By combining MAGIC with the DGRP, it is now possible to validate
238 causal effects of specific natural alleles in cellular or developmental processes in a tissue-
239 specific manner. The DGRP can also be used in MAGIC-based genetic screens to identify
240 natural alleles that, when made homozygous, can cause or modify certain phenotypes.
241 Importantly, MAGIC can in theory be utilized in a wide array of organisms that are compatible
242 with CRISPR/Cas9 (Harrison et al., 2014). In model systems that allow for transgenesis of
243 gRNA-marker constructs, such as mouse, zebrafish, and *Xenopus*, Cas9 can be introduced by
244 injection or virus transduction to further simplify genetic manipulations. Therefore, the flexibility
245 and power of mosaic analysis that are familiar to the *Drosophila* research community are now in
246 reach of researchers who study organisms which have not, or have rarely, been amenable to
247 clonal analysis.

248 **Materials and Methods:**

249 ***Fly Stocks and Husbandry***

250 See the Key Resource Table for details of fly stocks used in this study. Broadly, all fly lines were
251 either generated in the Han and Wolfner labs, or obtained from the Bloomington *Drosophila*
252 Stock Center or the *Drosophila* Genetic Reference Panel (MacKay et al., 2012). All flies were
253 grown on standard yeast-glucose medium, in a 12:12 light/dark cycle, at room temperature (22
254 ± 1°C, for the egg laying assay) or 25°C (for larval assays) unless otherwise noted. Virgin males
255 and females for mating experiments were aged for 3-5 days. Virgin females were aged on
256 yeasted food for germline clonal analysis.

257 To test germline clone induction, we combined *nos-Cas9* and ovo^{D1}, and then the gRNA
258 in two sequential crosses in schemes shown in Figure S1.

259 To visualize clones of C4da neurons, we used *ppk-Gal4 UAS-CD4-tdTom* (Figure 2) and
260 *ppk-Gal4 UAS-MApHS* (Figure 3, only the tdTom channel is shown).

261 ***Molecular Cloning***

262 *zk-Cas9:* The entry vector pENTR221-ZK2 (Poe et al., 2017) and the destination vector pDEST-
263 APIC-Cas9 (Addgene 121657) were combined in a Gateway LR reaction to generate the
264 expression vector pAPIC2-ZK2-Cas9.

265 *MAGIC gRNA-marker vectors*: gRNA-marker vectors were constructed similarly to pAC-U63-
266 tgRNA-Rev (Addgene 112811, Poe et al., 2019) but have either a ubi-nBFP (in pAC-U63-
267 tgRNA-nlsBFP) or a ubi-Gal80 (in pAC-U63-tgRNA-Gal80) marker immediately after the U6 3'
268 flanking sequence. The markers contain a Ubi-p63E promoter, mTagBFP-NLS or Gal80 coding
269 sequence, and His2Av polyA sequence. The Ubi-p63E promoter was amplified from *Ubi-*
270 *CasExpress* genomic DNA using the oligonucleotides
271 TTAATGCGTATGCATTCTAGTggccatggcttgctgttcttcgcgttc and
272 TTGGATTATTctgcgggcagaaaatagagatgtggaaaattag. mTagBFP-NLS was synthesized as a
273 gBlock DNA fragment (Integrated DNA Technologies, Inc.). Gal80 coding sequence was PCR
274 amplified from pBPGAL80Uw-4 (Addgene 26235) using the oligonucleotides
275 aaaaaaaaatcaaaATGAGCGGTACCGATTACAACAAAAGGAGTAGTGTGAG and
276 GCCGACTGGCTTAGTTAattaattctagaTTAAAGCGAGTAGTGGGAGATGTTG. The His2Av
277 polyA sequence was PCR amplified from pDEST-APLO (Addgene 112805). DNA fragments
278 were assembled together using NEBuilder DNA Assembly (New England Biolabs Inc.).

279 *gRNA expression vectors:* For *gnu* and *Rab3*, gRNA target sequences were cloned into pAC-
280 U63-tgRNA-Rev as described (Poe et al., 2019). For gRNAs targeting 2L, gRNA target
281 sequences were cloned into pAC-U63-tgRNA-nlsBFP and pAC-U63-tgRNA-Gal80 using
282 NEBuilder DNA Assembly. In the gRNA-marker constructs, the tRNA between the first and
283 second gRNAs is a *Drosophila* glutamine tRNA

284 (cagcgcGGTTCCATGGTGTAATGGTTAGCACTCAGGACTCTGAATCCTGCGATCCGAGTTCA
285 AATCTCGGTGGAACCT) instead of a rice glycine tRNA.
286 Injections were carried out by Rainbow Transgenic Flies (Camarillo, CA 93012 USA) to
287 transform flies through φC31 integrase-mediated integration into attP docker sites.
288 pAPIC2-ZK2-Cas9 and gRNA-marker constructs were integrated into the *attP*^{VK00037} site on the
289 second chromosome and expression vectors containing gRNAs targeting *Rab3* or *gnu* were
290 integrated into the *attP*^{VK00027} site on the third chromosome. Transgenic insertions were
291 validated by genomic PCR or sequencing.
292 ***Identification of gRNA target sequence***
293 gRNA target sequences for *Rab3* and *gnu* were identified as described previously (Poe et al.,
294 2019). Briefly, two gRNA prediction methods were used: sgRNA Scorer 2.0 (Chari et al., 2017)
295 (https://crispr.med.harvard.edu) and Benchling (www.benchling.com). Candidate target
296 sequences were those that obtained high on-target scores in both algorithms. CasFinder (Aach
297 et al., 2014) was used to identify and reject any sequences with more than one target site. Two
298 target sequences against coding exons for all splice isoforms were chosen for each targeted
299 gene. gRNA target sequences for 2L were identified by visually scanning through
300 pericentromeric sequences using UCSC Genome Browser (https://genome.ucsc.edu/) following
301 principles described in the Results section. The gRNA target sequences are listed in the table
302 below.

Gene	**Target sequence 1**	**Target sequence 2**
gnu	TTCGAATGTAAAAGCTTCGG	TTCCTGCCAACGCCTCCAGT
Rab3	GCCCACCGTGGAGACGAAGG	AGTGCGACATGGAGGACCAG
40D2	AGTCACCTGAAATAAGTCAG	GTTAGCCATCACAAGAACAG
40D4	GGGTTGTCTCCTGATATGGG	AACCGAACTGAACTCAACTG
40E1	CCGAATGATTTCATGTGAAG	TAGGGCAATTAAATATGTCA

303 ***Live Imaging of neurons***

304 Live imaging was performed as previously described (Poe et al., 2017). Briefly, animals were
305 reared at 25˚C in density-controlled vials for between 96 and 120 hours after egg-laying (to
306 obtain third to late-third instar larvae). Larvae were mounted in glycerol and their C4da neurons
307 at segments A1-A6 were imaged using a Leica SP8 confocal microscope with a 20x oil objective
308 and a z-step size of 3.5 μm.

309 ***Imaginal disc imaging***

310 Imaginal disc dissections were performed as described previously (Han et al., 2004). Briefly,
311 wandering third instar larvae were dissected in a small petri dish filled with cold PBS. The
312 anterior half of the larva was inverted and the trachea and gut were removed. The sample was
313 then transferred to 4% formaldehyde in PBS and fixed for 15 minutes at room temperature. After
314 washing with PBS, the imaginal discs were placed in SlowFade Diamond Antifade Mountant
315 (Thermo Fisher Scientific) on a glass slide. A coverslip was lightly pressed on top. Imaginal
316 discs were imaged using a Leica SP8 confocal microscope with a 20X oil objective.

317 ***Assays for Germline Clonal Analysis***

318 To monitor mitotic recombination events resulting in germline clone generation, we performed
319 egg-laying and egg hatchability assays as detailed in Hu and Wolfner (2019), with the exception
320 of using Canton-S males in place of ORP2 males as wild-type mates. Hatchability was
321 calculated only for females that laid eggs. Females that laid no eggs were eliminated from
322 hatchability calculations to avoid inflation of false-zero values.

323 ***Image Analysis and Quantification***

324 Counting of wing disc clones was completed manually in Fiji/ImageJ. Counting of neuronal
325 clones was completed manually during the imaging process.

326 ***Statistical Analysis***

327 Statistical analyses were performed in R. Student's t-test was conducted for egg-laying data
328 using *Rab* and *kni* gRNAs. For egg-laying data using the 2L toolkit, we performed estimated

329 marginal means contrasts between gRNAs and *post hoc* one sample t-tests using a generalized
330 linear model with a negative binomial response. For hatchability data using the 2L toolkit, we
331 performed estimated marginal means contrasts between proportions of hatched/non-hatched
332 eggs for each gRNA using a generalized linear mixed-effects model with a binomial response.
333 For all contrasts, p-values were corrected for multiple comparisons using the Tukey method. For
334 wing disc and neuronal clone data, we performed Welch's analysis of variance (ANOVA)
335 followed by pairwise *post hoc* Welch's t-tests. p-values from the multiple *post hoc* Welch's t-
336 tests were corrected for multiple comparisons using the Bonferroni method.

337 **Acknowledgments:**

338 We thank Bloomington *Drosophila* Stock Center (NIH P40OD018537) and the *Drosophila*
339 Genetic Reference Panel for fly stocks; Cedric Feschotte, Andy Clark, Eric Alani, and Marcus
340 Smolka for advice on gRNA design; Cornell CSCU consultants Stephen Parry and Erika Mudrak
341 for advice on statistics; Michael Goldberg and John Schimenti for critical reading and
342 suggestions on the manuscript. This work was supported by a Cornell start-up fund and NIH
343 grants (R01NS099125 and R21OD023824) awarded to C.H., an NIH grant (R01-HD038921)
344 awarded to M.W., and an NIH training grant (T32-GM07273) awarded to the Cornell BMCB
345 graduate program that supported S.A..

346 **References:**

347 Aach, J., Mali, P., and Church, G.M. (2014). CasFinder: Flexible algorithm for identifying specific
348 Cas9 targets in genomes (Cold Spring Harbor Laboratory).
349 Chari, R., Yeo, N.C., Chavez, A., and Church, G.M. (2017). SgRNA Scorer 2.0: A Species-
350 Independent Model to Predict CRISPR/Cas9 Activity. ACS Synth. Biol. *6*, 902–904.
351 Chen, S., Gendelman, H.K., Roche, J.P., Alsharif, P., and Graf, E.R. (2015). Mutational Analysis
352 of Rab3 Function for Controlling Active Zone Protein Composition at the Drosophila
353 Neuromuscular Junction.
354 Chou, T.-B., and Perrimon, N. (1992). Use of a Yeast Sitespecific Recombinase to Produce

355 Female Germline Chimeras in Drosophila.
356 Chou, T.-B., Noll, E., and Perrimon, N. (1993). Autosomal P[ovoD1] dominant female-sterile
357 insertions in Drosophila and their use in generating germ-line chimeras.
358 Chung, B.Y., Ro, J., Hutter, S.A., Miller, K.M., Guduguntla, L.S., Kondo, S., and Pletcher, S.D.
359 (2017). Drosophila Neuropeptide F Signaling Independently Regulates Feeding and Sleep-
360 Wake Behavior. Cell Rep. *19*, 2441–2450.
361 Clark, A.G., Silveriat, S., Meyerst, W., and Langleyt, C.H. (1994). Nature screen: An efficient
362 method for screening natural populations of Drosophila for targeted P-element insertions
363 (transposon tagging/reverse genetics/PCR/mutagenesis).
364 Clarkson, M., and Saint, R. (1999). A His2AvDGFP Fusion Gene Complements a Lethal
365 His2AvD Mutant Allele and Provides an in Vivo Marker for Drosophila Chromosome Behavior
366 (M ary Ann Liebert, Inc. Pp).
367 Feng, Y., and Irvine, K.D. (2007). Fat and Expanded act in parallel to regulate growth through
368 Warts. Proc. Natl. Acad. Sci. U. S. A. *104*, 20362–20367.
369 Freeman, M., Niisslein-Volhard, C., and Glover', D.M. (1966). The Dissociation of Nuclear and
370 Centrosomal Division in gnu, a Mutation Causing Giant Nuclei in Drosophila.
371 Garcia-Bellido, A., Ripoll, P., and Morata, G. (1976). Developmental compartmentalization in the
372 dorsal mesothoracic disc of Drosophila. Dev. Biol. *48*, 132–147.
373 Golic, K.G., and Lindquist, S. (1989). The FLP recombinase of yeast catalyzes site-specific
374 recombination in the drosophila genome. Cell *59*, 499–509.
375 Gratz, S.J., Cummings, A.M., Nguyen, J.N., Hamm, D.C., Donohue, L.K., Harrison, M.M.,
376 Wildonger, J., and O'connor-Giles, K.M. (2013). Genome Engineering of Drosophila with the
377 CRISPR RNA-Guided Cas9 Nuclease.
378 Grenier, J.K., Arguello, J.R., Moreira, M.C., Gottipati, S., Mohammed, J., Hackett, S.R.,
379 Boughton, R., Greenberg, A.J., and Clark, A.G. (2015). Global Diversity Lines-A Five-Continent
380 Reference Panel of Sequenced Drosophila melanogaster Strains.

381 Griffin, R., Sustar, A., Bonvin, M., Binari, R., Del Valle Rodriguez, A., Hohl, A.M., Bateman, J.R.,
382 Villalta, C., Heffern, E., Grunwald, D., et al. (2009). The twin spot generator for differential
383 Drosophila lineage analysis. Nat. Methods *6*.
384 Griffin, R., Binari, R., and Perrimon, N. (2014). Genetic odyssey to generate marked clones in
385 Drosophila mosaics.
386 Han, C., Belenkaya, T.Y., Wang, B., and Lin, X. (2004). Drosophila glypicans control the cell-to-
387 cell movement of Hedgehog by a dynamin-independent process. Development.
388 Hardwick, K.G., and Pelham, H.R.B. (1992). SED5 encodes a 39-kD integral membrane protein
389 required for vesicular transport between the ER and the Golgi complex. J. Cell Biol. *119*, 513–
390 521.
391 Harrison, D.A., and Perrimon, N. (1993). Simple and efficient generation of marked clones in
392 Drosophila.
393 Harrison, M.M., Jenkins, B. V, O'connor-Giles, K.M., and Wildonger, J. (2014). A CRISPR view
394 of development.
395 Heitzler, P., and Simpson, P. (1991). The choice of cell fate in the epidermis of Drosophila. Cell
396 *64*, 1083–1092.
397 Henner, A., Ventura, P.B., Jiang, Y., and Zong, H. (2013). MADM-ML, a Mouse Genetic Mosaic
398 System with Increased Clonal Efficiency. PLoS One *8*, 77672.
399 Hu, D.J.-K., and Jasper, H. (2019). Control of Intestinal Cell Fate by Dynamic Mitotic Spindle
400 Repositioning Influences Epithelial Homeostasis and Longevity. Cell Rep. *28*, 2807-2823.e5.
401 Hu, Q., and Wolfner, M.F. (2019). The Drosophila Trpm channel mediates calcium influx during
402 egg activation.
403 Huang, X., Shi, L., Cao, J., He, F., Li, R., Zhang, Y., Miao, S., Jin, L., Qu, J., Li, Z., et al. (2014).
404 The Sterile 20-Like kinase tao controls tissue homeostasis by regulating the hippo pathway in
405 drosophila adult midgut. J. Genet. Genomics *41*, 429–438.
406 Jinek, M., Chylinski, K., Fonfara, I., Hauer, M., Doudna, J.A., and Charpentier, E. (2012). A

407 Programmable Dual-RNA-Guided DNA Endonuclease in Adaptive Bacterial Immunity.
408 Lee, T. (2014). Generating mosaics for lineage analysis in flies. Wiley Interdiscip. Rev. Dev.
409 Biol. *3*, 69–81.
410 Lee, T., and Luo, L. (1999). Mosaic Analysis with a Repressible Neurotechnique Cell Marker for
411 Studies of Gene Function in Neuronal Morphogenesis.
412 Mackay, T.F.C., and Huang, W. (2018). Charting the genotype-phenotype map: lessons from
413 the Drosophila melanogaster Genetic Reference Panel. Wiley Interdiscip. Rev. Dev. Biol. *7*,
414 e289.
415 MacKay, T.F.C., Richards, S., Stone, E.A., Barbadilla, A., Ayroles, J.F., Zhu, D., Casillas, S.,
416 Han, Y., Magwire, M.M., Cridland, J.M., et al. (2012). The Drosophila melanogaster Genetic
417 Reference Panel. Nature *482*, 173–178.
418 Muller, H.J. (1928). The Production of Mutations by X-Rays.
419 Peng, Y., Lee, J., Rowland, K., Wen, Y., Hua, H., Carlson, N., Lavania, S., Parrish, J.Z., and
420 Kim, M.D. (2015). Regulation of dendrite growth and maintenance by exocytosis.
421 Perrimon, N. (1998). Creating mosaics in Drosophila. Int. J. Dev. Biol. *42*, 243–247.
422 Perrimon, N., and Gans, M. (1983). Clonal analysis of the tissue specificity of recessive female-
423 sterile mutations of Drosophila melanogaster using a dominant female-sterile mutation
424 Fs(1)K1237. Dev. Biol. *100*, 365–373.
425 Perrimon, N., Engstromt, L., and Mahowald, A.P. (1989). Zygotic Lethals With Specific Maternal
426 Effect Phenotypes in Drosophila melanogaster. I. Loci on the X Chromosome.
427 Poe, A.R., Tang, L., Wang, B., Li, Y., Sapar, M.L., and Han, C. (2017). Dendritic space-filling
428 requires a neuronal type-specific extracellular permissive signal in Drosophila. Proc. Natl. Acad.
429 Sci.
430 Poe, A.R., Wang, B., Sapar, M.L., Ji, H., Li, K., Onabajo, T., and Fazliyeva, R. (2019).
431 Mutagenesis Reveals Gene Redundancy and Perdurance in Drosophila. Genetics *211*, 459–
432 472.

433 Port, F., Chen, H.-M., Lee, T., and Bullock, S.L. (2014). Optimized CRISPR/Cas tools for
434 efficient germline and somatic genome engineering in Drosophila. Proc. Natl. Acad. Sci. *111*,
435 E2967–E2976.
436 Ren, X., Sun, J., Housden, B.E., Hu, Y., Roesel, C., Lin, S., Liu, L.P., Yang, Z., Mao, D., Sun,
437 L., et al. (2013). Optimized gene editing technology for Drosophila melanogaster using germ
438 line-specific Cas9. Proc. Natl. Acad. Sci. U. S. A. *110*, 19012–19017.
439 Salsman, J., and Dellaire, G. (2017). Precision genome editing in the CRISPR era.
440 Sander, J.D., and Keith Joung, J. (2014). CRISPR-Cas systems for editing, regulating and
441 targeting genomes. Nat. Biotechnol. Vol. *32*.
442 Satoh, D., Sato, D., Tsuyama, T., Saito, M., Ohkura, H., Rolls, M.M., Ishikawa, F., and Uemura,
443 T. (2008). Spatial control of branching within dendritic arbors by dynein-dependent transport of
444 Rab5-endosomes.
445 Shorter, J., Couch, C., Huang, W., Carbone, M.A., Peiffer, J., Anholt, R.R.H., and Mackay,
446 T.F.C. (2015). Genetic architecture of natural variation in Drosophila melanogaster aggressive
447 behavior. Proc. Natl. Acad. Sci.
448 Stern, C. (1936). Somatic Crossing Over and Segregation In Drosophlia melanogaster.
449 Thibault, S.T., Singer, M.A., Miyazaki, W.Y., Milash, B., Dompe, N.A., Singh, C.M., Buchholz,
450 R., Demsky, M., Fawcett, R., Francis-Lang, H.L., et al. (2004). A complementary transposon
451 tool kit for Drosophila melanogaster using P and piggyBac.
452 Xu, T., and Rubin, G. (1993). Analysis of genetic mosaics in developing and adult Drosophila
453 tissues.
454 Xu, T., and Rubin, G. (2012). The effort to make mosaic analysis a household tool.
455 Development.
456 Yu, H.-H., Chen, C.-H., Shi, L., Huang, Y., and Lee, T. (2009). Twin-spot MARCM to reveal the
457 developmental origin and identity of neurons. Nat. Neurosci. Vol. *12*.
458 Zong, H., Espinosa, J.S., Su, H.H., Muzumdar, M.D., and Luo, L. (2005). Mosaic Analysis with

459 Double Markers in Mice. Cell.

460

461 **Figures:**

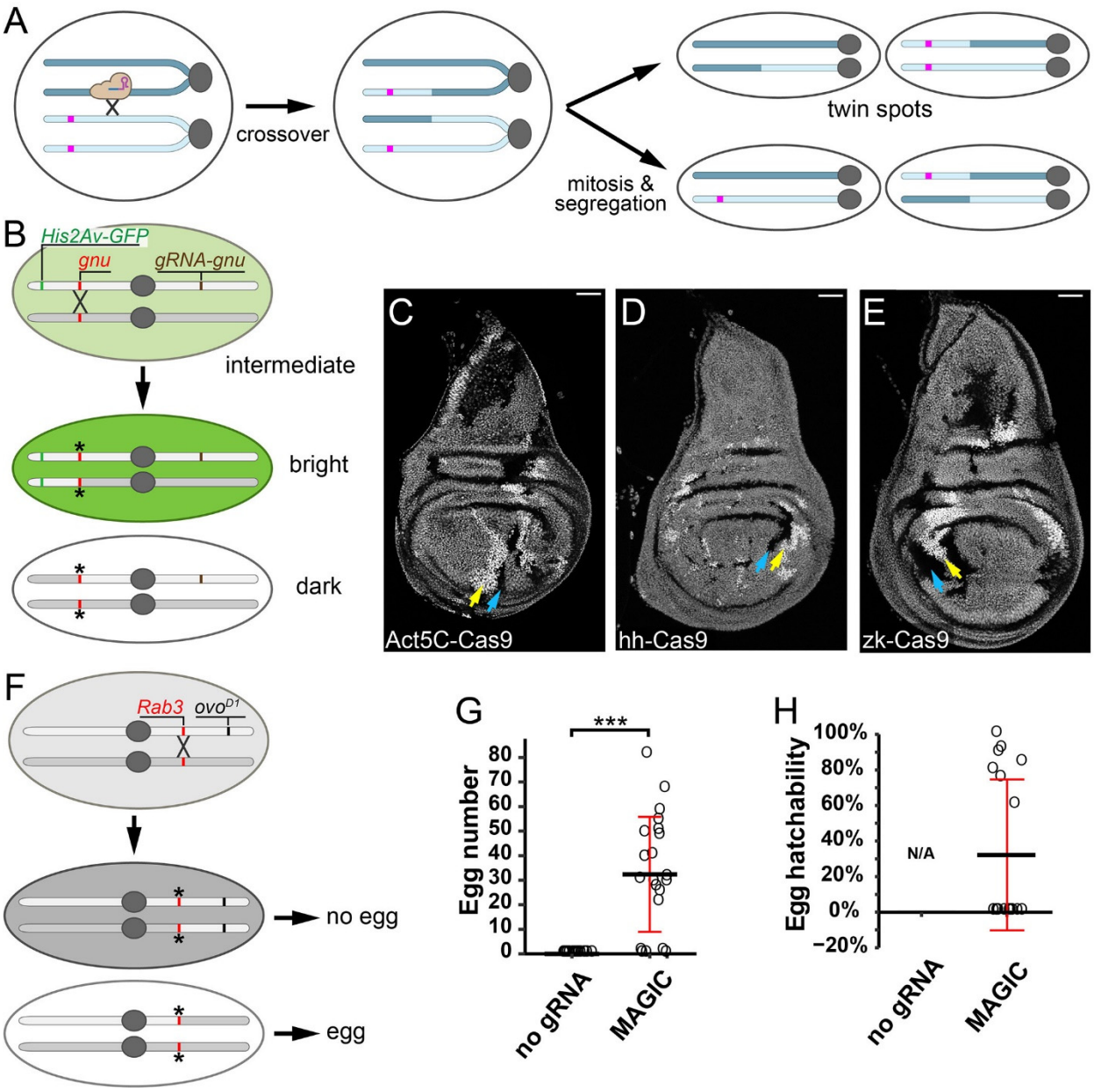

462

463 **Figure 1. CRISPR-induced crossover generates somatic and germline clones in**

464 ***Drosophila***

465 (A) A diagram illustrating how a CRISPR/Cas9-induced DSB leads to generation of
466 homozygous clones in a heterozygous organism. The magenta bar indicates an allele that
467 becomes homozygous in the twin spots.
468 (B) Strategy for generating mosaic clones using the *His2Av-GFP* marker and a crossover at the
469 *gnu* locus.
470 (C-E) Mosaic clones in wing discs visualized by levels of *His2Av-GFP* expression, as described
471 in the text. A pair of arrows indicate *His2Av-GFP*$^{+/+}$ (yellow) and *His2Av-GFP*$^{-/-}$ (blue) cells in
472 each panel. Clones were induced by *Act5C-Cas9* (**C**), *hh-Cas9* (**D**) and *zk-Cas9* (**E**). Scale bars,
473 50 μm.
474 (F) Strategy for generating and detecting clones in the female germline using *ovo*^{D1}.
475 (G) Number of eggs produced by females carrying *nos-Cas9* and *ovo*^{D1}, with (MAGIC) or
476 without (no gRNA) *gRNA-Rab3*. ***p<0.001, Student's t test. n=number females: no gRNA
477 (n=18); MAGIC (n=18).
478 (H) Hatchability of eggs produced females carrying *nos-Cas9* and *ovo*^{D1}, with (MAGIC) or
479 without (no gRNA) *gRNA-Rab3*. n=number females: no gRNA (N/A); MAGIC (n=18).
480 For all quantifications, black bar, mean; red bar, SD. Asterisks in (B) and (F) indicate mutated
481 gRNA target sites.

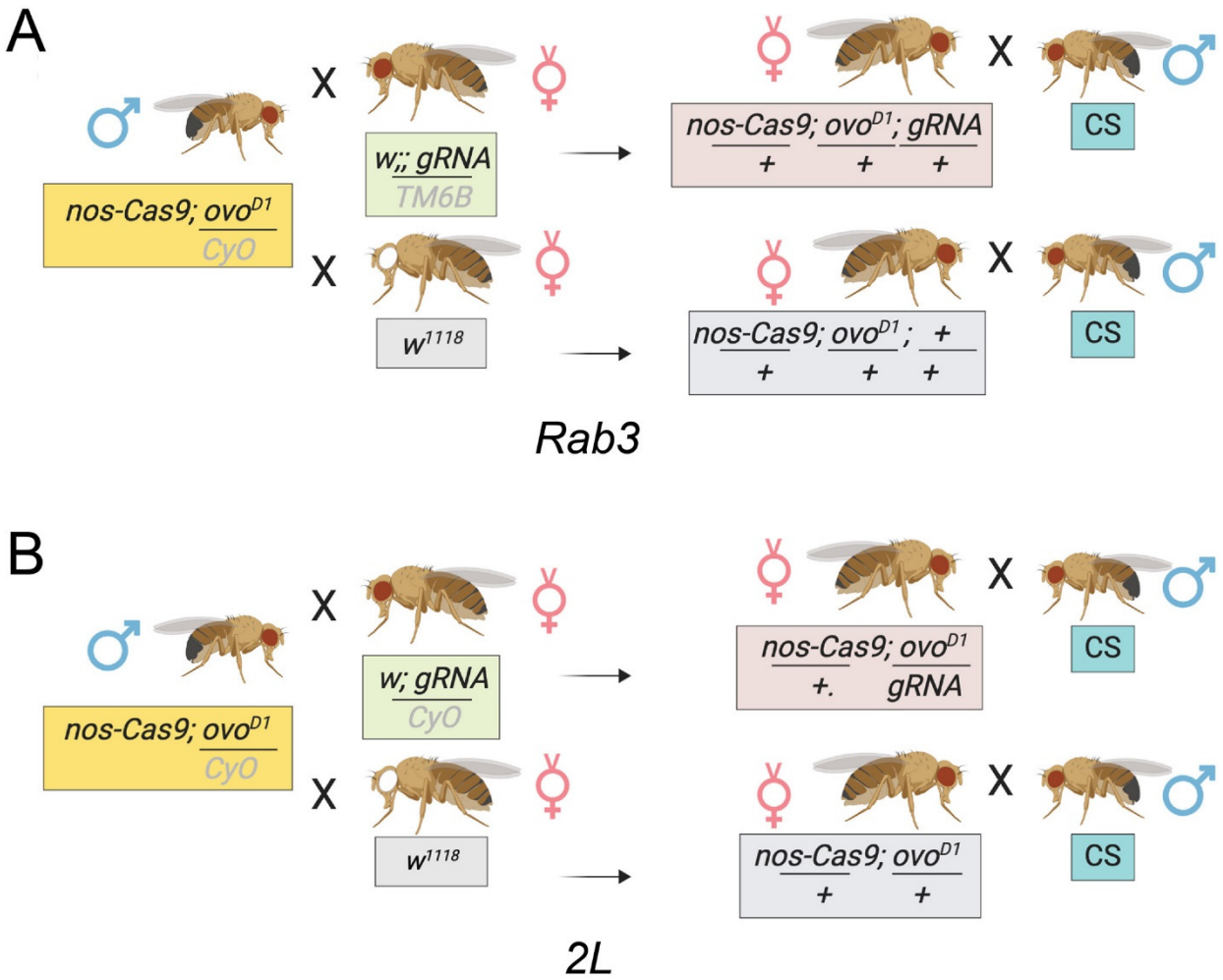

Figure S1. Crossing scheme for germline clone induction

(A) Crossing scheme for germline clone induction using *gRNA-Rab3*, *ovo*^{D1}(2R), and *nos-Cas9*.

(B) Crossing scheme for testing gRNAs for 2L in germline clone induction. The gRNAs used in this test were *gRNA(BFP)* lines.

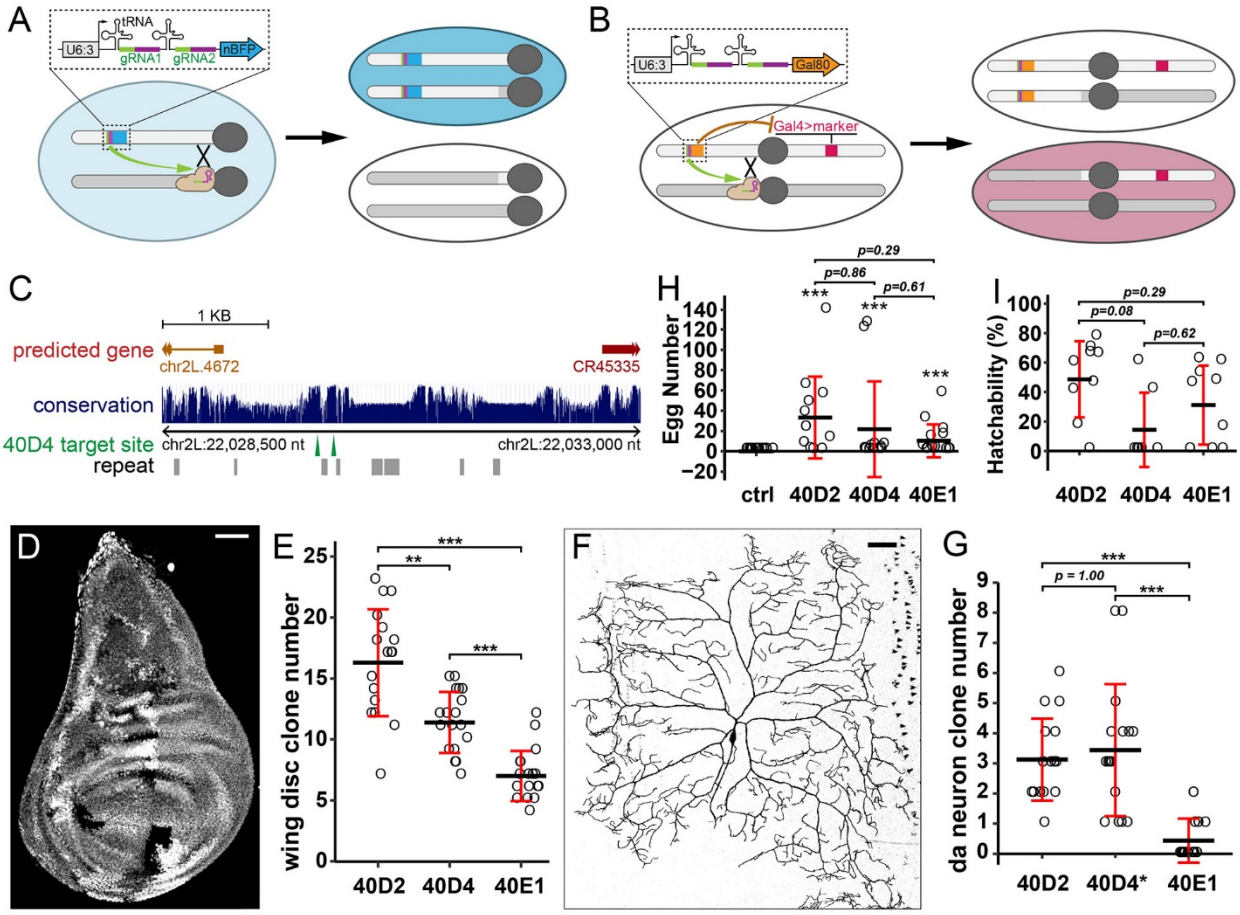

Figure 2. A toolkit for generating labeled clones for genes on chromosome arm 2L.

(A) Strategy for generating negatively labeled clones for genes on 2L using nuclear BFP.

(B) Strategy for generating positively labeled clones for genes on 2L using Gal80.

(C) A map for gRNA-(40D4) target sites derived from the UCSC Genome Browser. The height of the conservation bar corresponds to the level of conservation among 23 *Drosophila* species.

(D) A wing imaginal disc showing clones generated by a negative labeling construct (nBFP) paired with *hh-Cas9*.

(E) Number of clones in wing discs using three different gRNA(BFP) constructs. n=number of discs: 40D2 (n=17); 40D4 (n=18); 40E1(n=18). Welch's t-tests, p-values corrected using Bonferroni method; **p≤0.01, ***p≤0.001.

(F) A C4da neuron clone generated by a positive labeling construct (Gal80) paired with *SOP-Cas9* and *ppk>CD4-tdTom*.

500 (G) Quantification of C4da clones using three different gRNA(Gal80) constructs. n=number of
501 larvae: 40D2 (n=16); 40D4 (n=16); 40E1 (n=16). Clones were visualized by *ppk>CD4-tdTom.*
502 Welch's t-tests, p-values corrected using Bonferroni method; ***p≤0.001. The asterisk on 40D4
503 indicates frequent labeling of C3da clones.
504 (H) Number of eggs produced by using *ovo*^{D1}(2L), *nos-Cas9*, and three different gRNA(BFP)
505 constructs. The control (ctrl) has no gRNA. n=number of females: ctrl (n=13); 40D2 (n =12);
506 40D4 (n=12); 40E1 (n=14). Asterisks are from *post hoc* single sample t-tests that compare the
507 estimated marginal mean (EMM) of each gRNA against the control (μ = 0); ***p≤0.001. p-
508 values are from contrasts of EMMs of each gRNA (excluding control). EMMs are based on a
509 negative binomial model. All p-values were corrected using the Tukey method.
510 (I) Hatchability of eggs produced by females carrying *ovo*^{D1}(2L), *nos-Cas9*, and gRNA(BFP)
511 constructs. n=number female: 40D2 (n=9); 40D4 (n=7); 40E1(n=9). p-values are from contrasts
512 of EMMs of proportions of hatched/non-hatched eggs for each gRNA based on a binomial,
513 mixed-effects model and were corrected using the Tukey method.
514 For all quantifications: black bar, mean; red bar, SD. Scale bars, 50 μm.

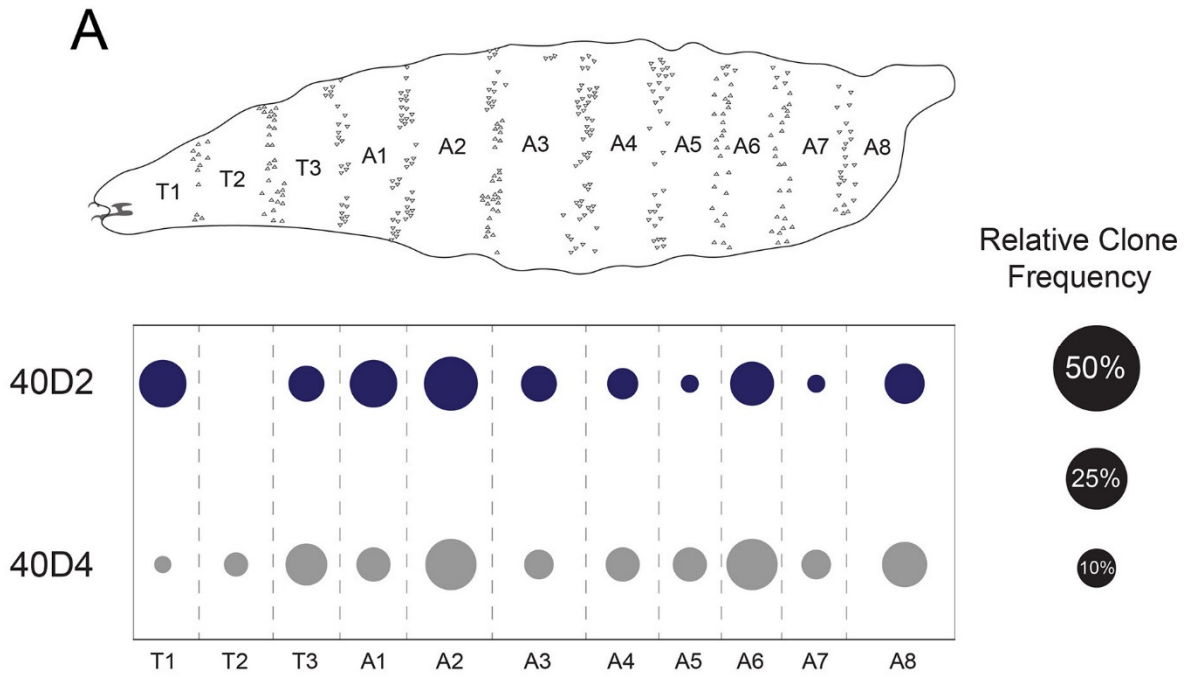

515

516 **Figure S2. Distribution of da neuron clones using gRNA(Gal80) for 2L**

517 (A) Distribution of da neuron clones in each segment using gRNA(Gal80) for 40D2 and 40D4.

518 n=number of neurons: 40D2 (n=47); 40D4 (n=52);

519 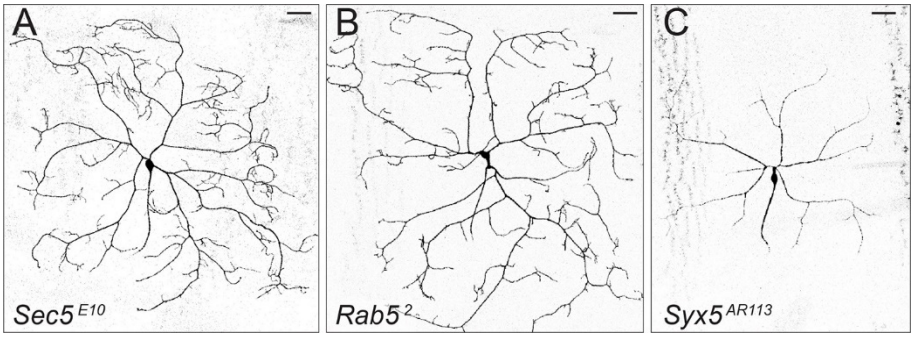

520 **Figure 3. Clonal analysis of example genes in neuronal dendrite development**

521 (A-C) MAGIC clones of C4da neurons using *Sec5*^{E10} (A), *Rab5*^{2} (B) and *Syx5*^{AR113} (C),

522 visualized by *ppk>MApHS*. Scale bars, 50 μm.

523 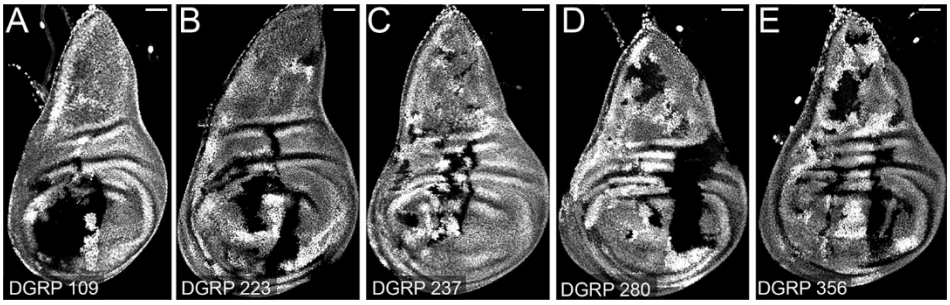

524 **Figure 4. MAGIC generates clones with DGRP lines**

525 (A-E) Clones in wing imaginal discs by pairing *gRNA-40D2(BFP); hh-Cas9* with DGRP line 109

526 (A), 223 (B), 237 (C), 280 (D) and 356 (E). Scale bars, 50 μm.

527

Key Resource Table

REAGENT or RESOURCE	SOURCE	IDENTIFIER	ADDITIONAL INFORMATION
Experimental Models: Organisms/Strains			
ppk-Gal4	Han et al., 2012		*ppk-Gal4* ^{VK00037}
ppk-Gal4	Han et al., 2012		*ppk-Gal4* ^{1A}
UAS-CD4-tdTom	Han et al., 2011	RRID:BDSC_35841	*UAS-CD4-tdTom* ^{7M1}
UAS-MApHS	Han et al., 2014		*UAS-MApHS* ^{VK00019}
His2Av-GFP	Bloomington Drosophila Stock Center	RRID:BDSC_5941	*His2Av-GFP(S65T)* ^{62A}
Act5C-Cas9	Bloomington Drosophila Stock Center	RRID:BDSC_54590	*Act5C-Cas9.P*
hh-Cas9	Poe et al., 2019		*R28E04-Cas9* ^{6A}
SOP-Cas9	Poe et al., 2019		*[sc-E1]x8-Cas9* ^{3A}
zk-Cas9	This study		*zk-Cas9* ^{VK00037}
nos-Cas9	Bloomington Drosophila Stock Center	RRID:BDSC_54591	*nos-Cas9.P* $^{ZH-2A}$
ovo ^{D1} *2L*	Bloomington Drosophila Stock Center	RRID:BDSC_2121	*ovoD1-18* ^{2La} *ovoD1-18* ^{2Lb}
ovo ^{D1} *2R*	Bloomington Drosophila Stock Center	RRID:BDSC_4434	*ovoD1-18* ^{2R}
gRNA-gnu	This study		*gRNA-gnu(U63)* ^{VK00027}
gRNA-Rab3	This study		*gRNA-Rab3* ^{VK00027}
gRNA-40D2(BFP)	This study		*w; gRNA-40D2(BFP)* ^{VK00037}
gRNA-40D4(BFP)	This study		*w; gRNA-40D4(BFP)* ^{VK00037}
gRNA-40E1(BFP)	This study		*w; gRNA-40E1(BFP)* ^{VK00037}
40D2(Gal80)	This study		*w; gRNA-40D2(Gal80)* ^{VK00037}
40D4(Gal80)	This study		*w; gRNA-40D4(Gal80)* ^{VK00037}
gRNA-40E1(Gal80)	This study		*w; gRNA-40E1(Gal80)* ^{VK00037}
gRNA-40D2(BFP)	This study		*w; gRNA-40D2(BFP)* ^{VK00037}
gRNA-40D4(BFP)	This study		*w; gRNA-40D4(BFP)* ^{VK00037}
Rab5 ^{2}	Bloomington Drosophila Stock Center	RRID:BDSC_42702	
Sec5 ^{E10}	Bloomington Drosophila Stock Center	RRID:BDSC_81044	
Syx5 ^{AR113}	Bloomington Drosophila Stock Center	RRID:BDSC_3645	
DGRP 109	Mackay et al., 2012	RRID:BDSC_28140	
DGRP 223	Mackay et al., 2012		
DGRP 237	Mackay et al., 2012		
DGRP 280	Mackay et al., 2012	RRID:BDSC_28164	
DGRP 356	Mackay et al., 2012	RRID:BDSC_28178	
Recombinant DNA			
pENTR221-ZK2	Poe et al., 2017		
pDEST-APIC-Cas9	Poe et al., 2019	RRID:Addgene_121657	
pAC-U63-tgRNA-Rev	Poe et al., 2019	RRID:Addgene_112811	
Ubi-CasExpress ^{attP40}	Bloomington Drosophila Stock Center	RRID:BDSC_65419	Genomic DNA used as a PCR template
pBPGAL80Uw-4	Addgene	RRID: Addgene_26235	
pDEST-APLO	Poe et al., 2017	RRID: Addgene_112805	

Key Resource Table

Software and Algorithms			
Fiji	https://fiji.sc/	RRID: SCR_002285	
R	https://www.r-project.org/	RRID: SCR_001905	
Adobe Photoshop	Adobe	RRID:SCR_014199	
Adobe Illustrator	Adobe	RRID:SCR_010279	
Other			
Gateway™ LR Clonase™ II Enzyme mix	Thermo Fisher Scientific,	#11791020	
NEBuilder® HiFi DNA Assembly Master Mix	New England Biolabs Inc.	#E2621	